RESEARCH PAPER

Modeling of stick-slip micro-drives

Christoph Edeler · Ingo Meyer · Sergej Fatikow

Abstract This paper describes substantial investigations on stick-slip micro drives. The drives are the basis for miniaturized micro- and nanohandling robots, which are usually driven by piezo-actuators. Because of the reason that stick-slip drives are strongly connected with friction characteristics of the stick-slip contact, this paper focuses on several aspects of friction and the model. After an introduction of former attempts to simulate stick-slip devices based on the so-called LuGre model, the CEIM friction model presented in this paper is based on the Elastoplastic-model. It is shown that one of the most significant phenomena, the "0-amplitude", is covered by the original Elastoplastic-model without modifications. Furthermore, a theoretic treatment of friction characteristics is performed. The properties of the model are validated by simulations and numerous measurements. Additionally, several adaptations are presented to enhance the model's capabilities. However, friction is a complex matter with manifold specificities. Thus, beside theoretic treatment, the center of gravity is also on "technical" issues to deliver not only an academic contribution to theory of friction, but to establish a tool for design and optimization of practical stick-slip positioners.

Keywords Piezo · Stick-slip · Model · Friction · Simulation · Elastoplastic · Micro-drive

C. Edeler (✉) · I. Meyer · S. Fatikow
Division Microrobotics and Control Engineering,
Uhlhornsweg 84, 26129 Oldenburg, Germany
e-mail: christoph.edeler@uni-oldenburg.de
URL: http://www.amir.uni-oldenburg.de

1 Introduction

In research and industry, the need for small and high-precision positioning devices is unchanged [1, 2]. A significant part of such positioners is covered by stick-slip devices, which are based on the periodical transportation (stick) and sliding (slip) of a runner driven by an actuating element [3–8]. These devices are characterized by a comparatively simple design consisting of few parts, backlash-free motion and very high resolution. This makes them attractive for building up small, cheap and accurate positioners. For this reason it should be due that such devices are in the focus of research. Indeed, there was a great concern in the nineties and in the following years. Numerous actuators and systems based on the stick-slip principle were published [9–20]. Though the focus was often on the proof of the individual concept, not on a deeper understanding of the stick-slip parameters. Nowadays interest seems to decrease. Only few research institutions worldwide deal with the investigation and development of stick-slip-based micro- and nanopositioners [21–25]. From the author's point of view, simulation and theoretic treatment of the stick-slip principle for microactuators were disregarded for several years. Therefore, this paper tries to make a contribution for the area of research on stick-slip modeling and simulation. It is outlined, which phenomena are of importance, and a model containing friction effects is introduced and discussed.

1.1 Objective and motivation of this paper

In most publications, stick-slip drives are not characterized by a theoretic model. It is simply assumed that the phases "Stick" and "Slip" alternate, which is true

most likely, but it is not an accurate description. In fact, an analysis of the conditions which lead to the change between the two phases is rarely given. In [26] the stick-slip mechanisms Abalone and NanoCrab are analyzed. Formulas are derived to calculate step length and control signal timing. The formulas are based on parameters, which are not further investigated. Comprehensive simulations were presented by a group of the EPFL, Switzerland [27–30]. They all have in common that they use the LuGre-model for simulation of friction, which is based on the interaction of the surface asperities of interacting bodies and was invented by authors in Lund and Grenoble [31]. A detailed introduction of the LuGre-model will be given in Section 2.1. As will be shown later on, the LuGre-model is capable to cover basic friction trend. Other effects known for a long time such as a minimum control amplitude for stick-slip actuators are not covered. Summarized, the following reasons account for an improved model of stick-slip friction:

– Stick-Slip devices for microrobots are usually designed as small as possible with dimensions of few mm^3. Additionally, the control signal contains very high slopes for the slipping. Therefore it is virtually impossible to measure the deformations directly.
– The prediction accuracy of recent simulation models is not sufficient for investigation of "minor" effects. The coarse function of the actuators is known (e.g. in the scale down to several decades of nm), but not effects of smaller scales.
– The design of virtually any stick-slip drive is based on empirical knowledge. Although basic coherencies are known, there is a lack of a model covering all important effects, such as the minimum control amplitude.
– Frequently stick-slip drives are explained by just two phases: The Stick and the Slip phase. Due to state-of-research friction theory, this has to be conceived as oversimplification [32].
– Effects such as a nonlinear actuator response [27] can not be explained. If piezohysteresis is the reason for that, it could be added to an all-embracing model.
– In practice it is often the case, that several stick-slip parameters influence each other, which makes investigation of individual parameters difficult. Or, uncertainty of friction occludes distinct effects. A model could be used to observe the influence of discrete parameters without uncertainties. Empirical measurements and friction theory have to be developed at the same time to complement each other.

– Using a model for design of Stick-Slip drives accelerates design process if the model is adequate enough.
– A correct friction model can be used to improve the actuator's response, e.g. to reduce or avoid vibrations.
– In the ideal case, a friction model takes into account not only empirical friction effects, but can explain the theory behind. Such effects could be influences of material parameters such as Youngs modulus. This would allow for further optimization. This is expected to be a great challenge.
– A model could be used not only to optimize the actuator, but also control electronics. As the slewrate affects the function of a stick-slip actuator or it's efficiency, respectively, an optimal (reduced) slewrate could enable cheaper control electronics [33].
– There is a demand for an accurate friction model to model and optimize friction-related methods such as open-loop force generation properly [34].
– Measurements become complicated for high control frequencies. A model is ideal to investigate effects occurring in this frequency domains.
– Acceleration and deceleration control can be easily tested using a simulation model (also see [8]). Likely this matter will be be of rising importance in the future for faster positioning in automation scenarios.

Summing up, there is need for an improved model based on friction theory and proven by measurements.
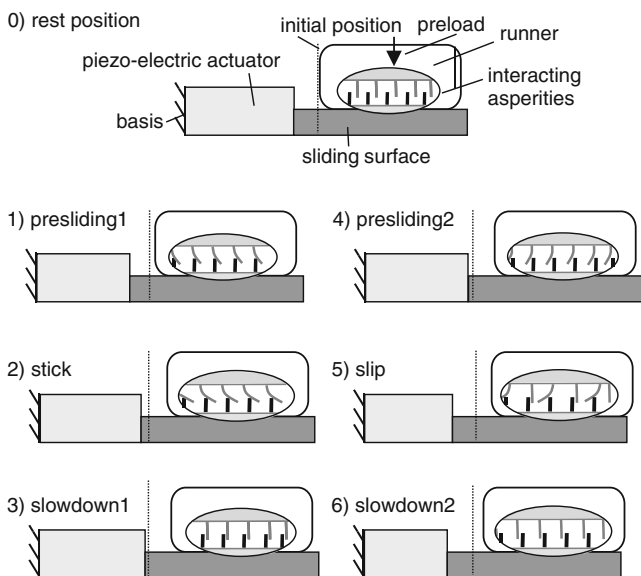
1.2 Organization of this paper

The paper is organized as follows: First of all, the principle of stick-slip positioning is presented for definition of general terms. At the same time the LuGre-model (LGM), and after that the Elastoplastic model (EPM) are introduced. Simulation runs are presented to show the capabilities of both models without extensions, and the results are compared with measurements. It is shown that several effects are not covered. Third of all a theoretic treatment is set in to discuss different "causes and effects" linked with friction and stick-slip conditions. A comparison with other attempts to explain friction developing from theory completes the insertion. Subsequently, modifications of the EPM are proposed to gain an improved model. The modified model again is evaluated by simulations and measurements. It is shown that major friction characteristics of the model have been modeled well. In Section 5.5 the CEIM-model as an adapted model for stick-slip simulation of micro devices is presented. Admittedly it is outlined

that several questions remain unanswered. Therefore, the paper closes with a summary and an outlook how to face remaining problems.

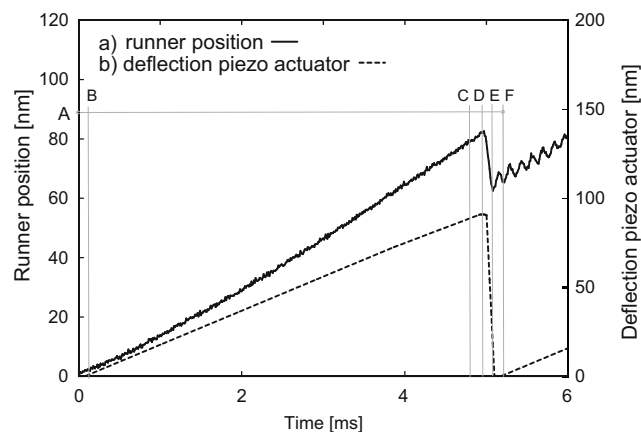## 2 Principle of stick-slip positioning

In this chapter, fundamental terms of stick-slip positioning technique are introduced. To illustrate the positioning process, a schematic sketch of a body positioned by an actuated sliding surface can be found in Fig. 1. A simplified treatment of the stick-slip process leads to the phases Slip and Stick. Figure 1(0) shows the rest position, Fig. 1(2) the Stick and Fig. 1(5) the slip state. For many applications, where stick-slip is an effect of minor meaning or even unwanted, this treatment is sufficient. However, for precision positioning a more detailed examination is necessary. According to theory of surface mechanics, the contact of two bodies with moderate normal force results not in a flat, continuous contact, but the surface asperities are in contact only [35]. Every single asperity exhibits mechanical properties such as compliance and dynamical progress. As a result, the interacting asperities add dynamic characteristic to a mechanical system, which can not be ignored for pre-

cise positioning on the micro- and nanometer scale. Figure 2 shows a typical excitation signal of a sawtooth shape. The slope is constant at the beginning (stick, point A to D). If a distinct **amplitude** of deflection is reached, a rapid movement in the opposite direction follows (slip, point D–F). This slip phase with high slope, further called **slewrate**, is essential for the function of micro stick-slip drives. The **sign** of the amplitude defines the direction of movement. The repetition rate of this signal mainly specifies the average velocity of the runner, it is further called stick-slip **frequency**. Different configurations of the excitation motion are thinkable, e.g. adding discrete steps [29]. More on that later on, for the moment we will concentrate on the signal defined by these four parameters.

Additionally, Fig. 2 shows a position graph of a runner's response. The sliding surface (according to Fig. 1) was excited by a piezoelectric actuator controlled by sawtooth signal. More details on the stick-slip axis and the testbed can be found in [33]. Apparently the measured position signal can be obtained as a typical example, given that signal responses of other devices look almost the same [27]. The parameters for generation of the position signal in Fig. 2 are presented in Table 1. Although an ideal run cannot be expected, several distinct divergences can be observed. First, the amplitude of the excitation just before the slip is not fully reached by the runner. Second, the run of the stick is not linear, which is an indicator for **nonlinear effects**. Third, there is a position change during the slip,

Fig. 1 Different states of a stick-slip positioning process, showing a body on an actuated sliding surface. The simplified stick-slip process consists of three phases: Rest position (*0*), stick phase with transport of the body (*2*) and slip phase with distinct relative movement of the body and the surface (*5*). According to the friction models based on surface mechanics, more phases can be identified: Oscillations subdivided into presliding (*1* and *2*) and slowdown (*3* and *6*), which finally result in rest position (not initial position). Preload is induced by the runner's weight in this example

Fig. 2 Sawtooth excitation signal (**a**) and runner's response (**b**). The response signal can be subdivided into the following phases, analogously to Fig. 1: Transition from initial position to stick (point *A–B*), stick phase (*B–C*), transition between stick and slip with deceleration of the stick movement (*C–D*, for better visualization *C* is drawn clearly in the stick-phase), slip with back-step (*D–E*) transition between slip to second stick (*E–F*). After point *F*, damped vibration can be observed. For further explanations, see text

Table 1 Typical parameters of the stick-slip device [33]

Name	Typ. value	Poss. range	Unit
Amplitude	300	$0 - V_{depol.}$	V_{PP}
Actuator disp.[a]	160	0–160	nm
Step size	130	<10–150	nm
Frequency	100	1–100 k	Hz
Slewrate	100	50–1,000	$\frac{V}{\mu s}$
Backstep	30	<10–100	% of step
Vibration freq.	4 k	Unknown	Hz
Vibration damp.	Unknown	Unknown	$\frac{Ns}{m}$
Runner's mass	4	3–15	g
$\sum F_{normal}$	0.4	0.25–20	N

[a]On the basis of simulations and indirect measurements

followed by some vibration. This **backstep** (D–E) is an indicator, that the slip phase must contain "non-slip" parts induced by the friction force. It will be shown that the backstep is influenced by material and normal force conditions. The **vibrations** after the backstep can be observed for virtually all micro stick-slip devices. They can be characterized by vibration frequency and damping rate. In this case, vibration frequency will be likely caused by the asperity-runner system and not by a compliant piezoactuator (this is supported by the measurement in Fig. 11, where the first eigenfrequency of the piezoactuator is determined to be at least two orders of magnitude higher than the vibration in Fig. 2). Finally, the system reaches rest condition during the following stick phase. Again, a nonlinear characteristic can be observed. It can be concluded that the real behavior of a stick-slip device is characterized by many different effects, which likely influence each other. In the next subsection, a short description of the state of research on the simulation of such stick-slip response is given.

2.1 Stick-slip simulation using the LuGre model

As indicated in the introduction, few researchers currently work on the investigation of stick-slip actuators. Some papers deal with modeling of rough surfaces, but not with respect to micro robotics [36]. The last widespread investigations were made by the group around Breguet [27]. Since then, no development of the used model is known to the authors of this paper. For this reason that work is the basis for the model presented in this paper.

Breguet selected the LGM for simulation of a linear stick-slip actuator. It is based on the interaction of surface asperities of interacting bodies [31]. The history of the LGM lies in modeling of friction effects in

"macro" machines. Of course, in macro scale other friction effects dominate than in micro scale. E.g., viscous friction is observed typically for lubricated contacts with large differential velocities between the sliding surfaces. It will be shown that some effects do not play a role in micro devices.

The LGM is a single-state friction model. For this reason a differentiation between several states, such as Sticking or Slipping with changing conditions is needless (in severe friction models, different states are toggled. This can be the reason for further difficulties [37]). The model's reaction is dominated by the lumped average deflection of the surface asperities.

Hence, this makes the LGM attractive for easy simulation implementation. The fundamental formulas are repeated here for further discussion, although they can also be found in [31]. Equation 1 shows the coherency of the friction force in relation to the average asperity deflection z and its derivative $\dot{z}$:

$$F_{friction} = \sigma_0 \cdot z + \sigma_1 \cdot \dot{z} + \sigma_2 \cdot v_{diff}. \tag{1}$$

Apart from z, friction force is defined by the three parameters σ_0, σ_1 and σ_2. z represents the average asperity deflection and $\dot{z}$ its derivative. For easy discrete simulation, integrative progress is preferred to derivative one. Therefore, z is calculated from $\dot{z}$:

$$z = \int \dot{z} \, dt. \tag{2}$$

Calculation of $\dot{z}$ comprises the deflection developing of the asperities

$$\dot{z} = v_{diff} - \frac{|v_{diff}|}{g(v_{diff})} \cdot z, \tag{3}$$

including dependency on velocity (Stribeck curve) and compliance of the asperities σ_0

$$g(v_{diff}) = \frac{F_{stribeck}(v_{diff})}{\sigma_0}. \tag{4}$$

The combination with a simple mechanical model, consisting of an accelerated mass afflicted with inertia results in

$$m_{runner} \cdot \ddot{x} = F_{friction}, \tag{5}$$

with

$$v_{diff} = \dot{x} - \dot{u}, \tag{6}$$

where u represents the excitation signal and $\dot{u}$ its accordant derivative. It can be concluded that the idea of representing the asperities' dynamical progress leads to a first-order differential equation as in Eq. 1. Combined with the mechanical system (Eq. 5) containing

a second-order term, a system capable of performing damped oscillations is created.

As Breguet showed, the run as in Fig. 2 can be qualitatively represented by the LGM. On the contrary important characteristic can not be represented by the LGM, namely the phenomenon that low amplitudes do not cause a slip or a measurable step length, respectively. This will result in an oscillation of the runner without step generation. Several investigations on this matter can be found in [33]. Thus, the largest control amplitude which does not generate a measurable step is further called **0-amplitude** (zero-amplitude). This 0-amplitude was observed by several authors. Breguet called it the "limit of contact deformation" x_s. He also presents a theoretic derivation [27]. Mariotto shows measurements of the step size dependent to control amplitude [38]. The authors of this paper also observed the effect [39]. Driesen states that excitation force does not overcome friction (Fig. 4.24 in [30]).

Figure 3 shows the coherency between step size and excitation amplitude for an idealized stick-slip actuator, the simulated step size using the LGM and measured step sizes of a miniaturized stick-slip drive. In the ideal case, there will be a proportional ratio between excitation amplitude and step size. The LGM shows a nonlinear, asymptotic progress, however, small amplitudes still cause steps in simulation. In contrary, the measured step sizes exhibit a distinct "dead zone" starting at zero amplitude. Interestingly, this effect seems not to be investigated for a certain time. Indeed there is the question, what the cause for the 0-amplitude is and how
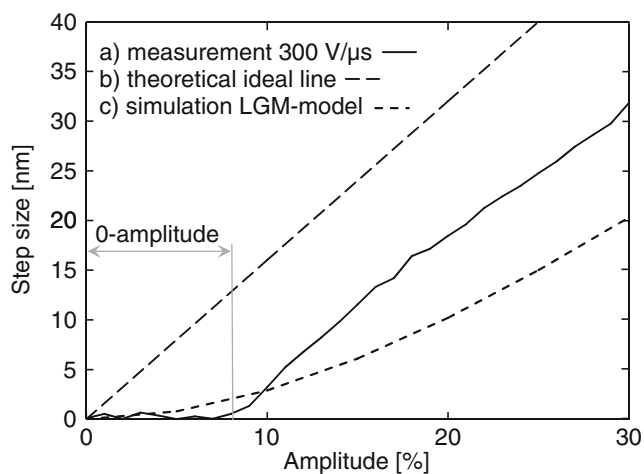
it can be modeled. In Sections 4.1 and 4.1.7 different contributing portions of the 0-amplitude are discussed.

2.2 Results of the LGM-based simulation

After all, the modeling results using the LGM based on the work of Breguet are:

– The static friction coefficient μ_s (based on Coulomb' friction) has less influence on the simulation results. Contrarily, dynamic friction coefficient μ_d can be used to "adapt" simulation results to measurements.
– The velocity-dependent Stribeck characteristic has no influence. Therefore, velocity-dependence can be neglected.
– Viscous friction can be neglected. Concretely, this results in a low value of σ_2.
– The tangential compliance σ_0 is of less importance. This is true for simulations of step length (Breguet showed this). But, this parameter can become very important for simulation of force generation [34].
– Damping of the vibrations occurring after the slip is critical for the function of the drive. For reliable operation, damping coefficient of the whole system must be large enough to reduce vibration significantly before the subsequent slip is executed.
– A short slip time or a higher slewrate, respectively, results in larger step size.
– Increased normal force in the stick-slip contact leads to reduced step size.
– Dynamic properties of the piezoactuators (such as mechanical stiffness and also damping) play an important role. However, as our piezoactuators can be treated as very stiff, we focus on stick-slip-drives with such actuators (see also Section 4.5).

A more detailed discussion about these issues will be given in Section 4. In the following section it will be shown that the Elastoplastic-model can cover at least the trend of 0-amplitude.

3 Stick-slip simulation using the elastoplastic model

The "elasto-plastic" model (EPM) was introduced a decade ago [40, 41]. It combines several properties in a single-state friction model:

– Presliding displacement, which is caused by tangential compliance [42],
– differentiation between the type of motion considered as "elastic" and "plastic" and both ("mixed"),
– stiction,

Fig. 3 Different trends of step size development against excitation amplitude. In the ideal case, there is a proportional ratio. The LuGre-model produces a *quadratic curve*. This is in contrast to the measured actuator, which exhibits a distinct zone of zero step size

– Stribeck friction curve,
– Coulomb and viscous friction,
– frictional memory and
– rising static friction.

The presence of elastic and mixed deformation is the difference to the LGM. Physically, the EPM covers unchanging friction forces without body's drift. E.g., a vertical runner hold in position by friction force exposured to small vibrations in the LGM always drifts due to gravity-caused presliding. In the EPM, friction force can be covered by stiction up to a certain amount due to breakaway-distance and therefore, the body will remain in position. Mathematically, Eq. 3 of the LGM changes in the EPM to

$$\dot{z} = v_{\text{diff}} - \frac{\alpha_{\text{transition}}() \cdot |v_{\text{diff}}|}{g(v_{\text{diff}})} \cdot z, \tag{7}$$

where $\alpha_{\text{transition}}()$ depends on z, z_{ba} and z_{ss} and decides whether the model behaves plastical or elastical or both (An explanation of these values will be given shortly). If $|z| < z_{\text{ba}}$, $\alpha()$ equals zero (pure elastic deformation) and if $|z| \geq z_{\text{ss}}$, $\alpha()$ equals one (pure plastic deformation as in the LGM). In the case if $z_{\text{ba}} \leq |z| \leq z_{\text{ss}}$ (mixed deformation) a transition function between zero and one applies. The function and a plot can be found in [41]. The transition function expresses the smooth transition between the states elastic and plastic deformation. But, by experience it is much more important by *what* the states of $\alpha_{\text{transition}}()$ change or which values are represented by z_{ba} and z_{ss}, respectively. The **breakaway distance** z_{ba} defines to which extend the asperity deflection (beginning from zero) can be treated as elastic. A deflection of z between z_{ba} and z_{ss} exhibits both elastic and plastic deformation. z_{ss} stands for the maximum average deflection of the asperities for constant v_{diff} in a **steady state** ($z_{\text{steadystate}}$). Finally, deformations above z_{ss} are characterized by plastic deformation. Because of this reason values of z_{ba} and z_{ss} are crucial for the representation of effects such as the 0-amplitude. Currently, the idea is to bring together the empirical gathered value of 0-amplitude and the elastoplastic progress of the EPM. A first implementation with the values $z_{\text{ba}} = 50$ nm and $z_{\text{ss}} = 100$ nm leads to the simulated step lengths as in Fig. 4b. The curve is comparable qualitatively to the measurement in Fig. 3a, although only few parameters were adapted. Ratios between z_{ba} and z_{ss} strongly differing from 50% show a tendency either to generate negative steps (Fig. 4c) or increased 0-amplitude (Fig. 4a). The effect of negative steps is here treated as a simulation side-effect, which is not of interest for the following simulations. Nevertheless, negative steps could be interpreted as steps,
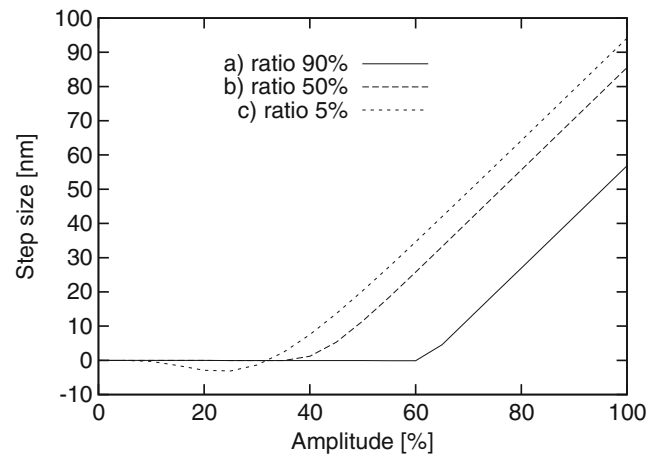

Fig. 4 Simulated steps sizes using the EPM, **a** ratio between z_{ba} and $z_{\text{ss}} = 90\%$, **b** ratio of 50% and **c** ratio of 5% (see text)

where no real slip occurs and the negative deformations during the transitions dominate. Finally, 0-amplitude can be seen as the very empirical value, which describes the theoretic transition between pure elastic and mixed elastoplastic deflection characteristics.

Another important parameter of stick-slip drives is the normal force applied in the stick-slip contacts, further called **preload** (see also Fig. 1). It is generally known from literature that the devices are sensitive to preload. If preload is too low, stick will not function and the runner's transportation or guiding, respectively, fails. In the opposite case a high preload prevents the device to enter Slip. The result is a runner oscillating around its initial position. Figure 5 shows a measured curve ("steel measured") of the step size caused by different preload and three attempts to simulate the matter, the LGM, and twice the EPM with two different approaches to define z_{ba} and z_{ss}: The first scenario (EPM $z_{\text{ss,calc}}$) takes over the calculation of z_{ss} from other model variables. The resulting range of z_{ss} shown in Table 2 is calculated as

$$z_{\text{ss}} = \frac{F_{\text{stribeck}}}{\sigma_0} = g(v_{\text{diff}}). \tag{8}$$

z_{ba} is fixed (arbitrarily user-defined). In the second scenario (EPM $z_{\text{ss,fix}}$) the calculation of z_{ss} is replaced by a fixed, user-defined value. As a result, no model is able to reproduce the measured preload-dependent developing, which is distinguished by a proportional reduction of step size with increasing preload. At a certain point (approximately 5 N in Fig. 5), step size reaches and remains zero. In contrast to the measurement no model reaches zero step size. In fact, all models show an asymptotic run, but with different conditions for small
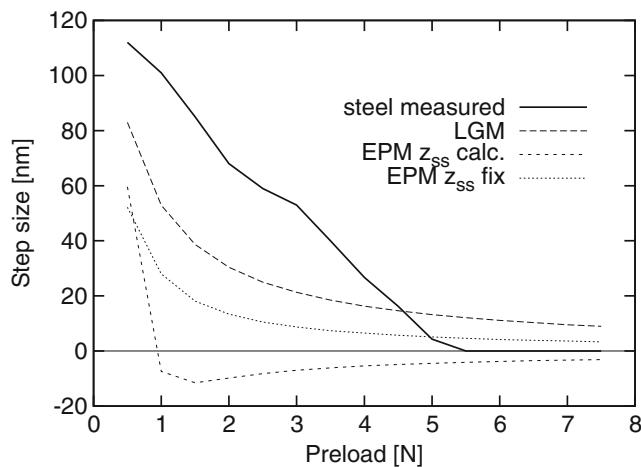
Fig. 5 Simulation and measurement of the preload-dependent progress. Three simulation model developings are shown in comparison to the measured trend of steel: The LGM, the EPM with calculated z_{ss} and the EPM with fixed z_{ss} (see text). Simulation parameters can be found in Table 2

preload. The LGM and the $EPM_{zss,fix}$ show similar behavior but with different quantitative values. $EPM_{zss,calc}$ exhibits completely different trend with negative steps for preload above 1 N.

Obviously, neither the LGM nor the EPM cover the preload-dependent trend. This is likely caused by several reasons: The simulation parameters shown in Table 2 are not optimized for best result. This specially applies for σ_0, μ_s and μ_k. Furthermore $F_{preload}$ is not derived theoretically until now, which could lead to distorted trends. In the simulation $F_{preload}$ represents all real normal forces of the divers stick-slip contacts. But, early simulations showed that z_{ba} and z_{ss} have by far the most influence. As far as the maximum amplitude

Table 2 Simulation parameters of the models presented in Fig. 5

Parameter	LGM	EPM_{calc}	EPM_{fix}	Unit
σ_0	$1 \cdot 10^6$	$1 \cdot 10^6$	$1 \cdot 10^6$	$\frac{N}{m}$
σ_1	5	5	5	$\frac{Ns}{m}$
σ_2	0	0	0	$\frac{Ns}{m}$
μ_s	0.3	0.3	0.3	
μ_k	0.2	0.2	0.2	
m_{runner}	0.003	0.003	0.003	kg
$v_{Stribeck}$	0.001	0.001	0.001	$\frac{m}{s}$
z_{ba}		100	50	nm
z_{ss}		450–600[a]	100	nm

[a]Values calculated by Eq. 8, see text

of the measured stick-slip actuators is concerned (see Table 1), z_{ss} must be smaller. This is in contrary to the calculated value given in Eq. 8. A different way of deriving z_{ss} has to be found in order to match the measured characteristic. At the same time z_{ba} is assumed to define the progress as shown in Fig. 4. As far as z_{ba} must be smaller than z_{ss} to ensure a stable model simulation, a ratio of 50% seems to be the best choice. The relation of z_{ba} and z_{ss} will be discussed in detail in the following chapter.

It can be concluded that the EPM is able to reproduce 0-amplitude due to the elastic and mixed deflection. Though preload developing can not be expressed by any of the presented model configurations. Therefore some adaptations to the EPM are presented in Section 5 to face the defects. Due to the reason that influence of friction is by far the most important parameter of stick-slip micro drives, a theoretic treatment of the friction background is given now.

4 Theory behind stick-slip

Generally, modern friction theory is a large area of research which goes back at least several decades [32, 35, 43–50]. Particularly, investigations based on stick-slip theory cover an area reaching from earthquake research [51] via macro robotics [52] to nanoscale friction tribology [53, 54]. Many friction models exist, best choice of friction model is difficult. Theoretic models tend to be universal, at the same time they cannot explain side-effects. Empirical models are mostly conform to measurements. On the contrary it is hard to find theoretic explanations. As already indicated, investigations on micro stick-slip devices are rare, same applies for adequate friction models. Essential works were already cited within this paper. As a result, the LGM was state-of-research in modeling such devices.

There is still a gap between empirical measurements and friction theory using the LGM or the EPM. In this section it is tried to give a contribution to close this gap. Several effects, analogously to the following subsections, are discussed.

4.1 Causations of 0-amplitude

In the preliminary section it was shown that the EPM can cover the 0-amplitude qualitatively. In this paragraph it will be shown that the measured 0-amplitude equates to the break-away distance z_{ba} in the EPM. The latter has to be understood as the culmination of several elastic effects. However there is the question, what the

relation between presliding and 0-amplitude in both models is. For LGM, presliding is always present, i.e. forces below F_{static} formally do not change the runner's state to sliding, but cause a persistent displacement in the micro scale. Therefore, **forces** mainly determine model performance. Implicitly the LGM supports dissipative or both mixed and plastic deformation, respectively. Therefore, any (low) force will cause presliding and finally measureable step length (net displacement). Presliding will also cause vibrations. Mathematically, $\alpha_{transition}()$ equals one in the LGM (compare Eqs. 3 and 7), which conforms to pure plastic deformation.

In EPM presliding is subdivided into several cases. The parameters z_{ba} and z_{ss} with dimension "length" decide which developing is needed, elastic, mixed or plastic deformation. Therefore, EPM can be seen as a model defined by **distances**. In contrast to LGM, e.g. pure elastic deformation without plastic parts is enabled. The border between elastic deformation or zero step length, respectively, is defined by z_{ba}. Therefore, it is the corresponding value to 0-amp. Furthermore, if the exact amplitude of the exciting actuator is known, 0-amplitude and z_{ba} can be converted.

Theoretically, any elastic characteristic in the Stick-Slip-system will likely contribute to the amount of 0-amplitude. Therefore, the measured 0-amplitude is a mixture of several elastic effects. Friction pair is one important part, compliance of piezoactuator is another, other causations can be e.g. elastic hinges (glue connections).

4.1.1 Stiction and presliding

LGM does not cover stiction (short form for static friction, see also [40]), because the dissipative part $\dot{w}$ is always present. Hence, there is no pure elastic deformation. At this moment, the scale in which the models are applied becomes of interest. In macro scale (where the "origin" of LGM and EPM is located) a small net displacement coming with the LGM is of less interest. The focus used to be on the modeling of presliding (or presliding oscillation). In micro scale the unavoidable net displacement is in crass contrast to measurements (see Fig. 3). Admittedly presliding oscillations are observed.

What can be called presliding, is a question of definition: If presliding means the total return of the runner, only the state of elastic deformation can be treated as presliding (**elastic presliding**). If presliding means the general deformation under an exciting force, at least the mixed deformation has to be counted to presliding (**mixed presliding**). The "historical" definition of presliding is simple: A small displace-ment of a body caused by an external force with respect to "rough" contact. Under the current circumstances, definition of presliding could be reviewed.

As a matter of fact, in the 0-amplitude we have found the corresponding value to z_{ba}. In other words, z_{ba} can be **measured** using the 0-amplitude. The question comes up what defines 0-amplitude, which elements of a stick-slip device can exhibit both elastic, plastic or mixed conditions? The following list tries to collect probable reasons:

- Material conditions (Youngs modulus, hardness and abrasiveness, surface roughness, adhesive forces),
- mechanical compliances (glue connections, guiding),
- actuator properties (here: piezohysteresis) and
- other unknown reasons (temperature, humidity, et cetera).

It is obvious that many different reasons potentially influence 0-amplitude. Therefore, the effort to measure significant effects is tremendous. Hence, we will focus on two measurements which have been achieved yet.

4.1.2 Youngs modulus of the runner

The first investigated parameter is the Youngs modulus of the runner. The corresponding material of the actuator is ruby and remains unchanged. Several different materials with a large bandwidth of Youngs modulus from 70 to 600 N/mm^2 were chosen, as Table 3 shows. A measurement of the individual resulting 0-amplitude is shown in Fig. 6. Obviously stiffer materials rather tend to plastic deformation: the breakaway distance or the 0-amplitude, respectively, decreases with rising Youngs modulus. Thus, the bonding mechanisms are weaker for higher stiffness. An alternative explanation could be found in Hertzian contact theory [55]. Every element in contact with the runner causes an imprint

Table 3 Selected runner materials

Material	Youngs mod. [kN/mm^2]	Comment
Glass	70[a]	Object holder
AlMgSi0.5	70	EN AW 6060
CuZn39Pb3	97	Brass alloy
Steel	200	1.4301
Steel	215	1.4112, HRW 55
Steel pin	220	DIN 6325
Al$_2$O$_3$	350	Ceramic (white)
Tungsten	400	Welding electrode
Tungsten carbide	600	Low-wear tool

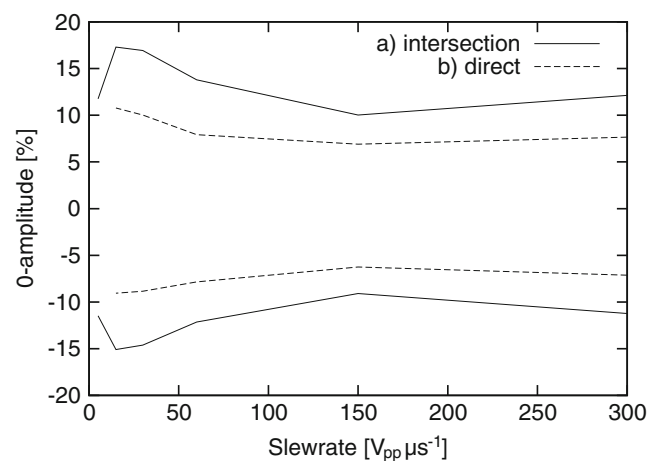[a]Highest value of 0-amplitude in Fig. 6
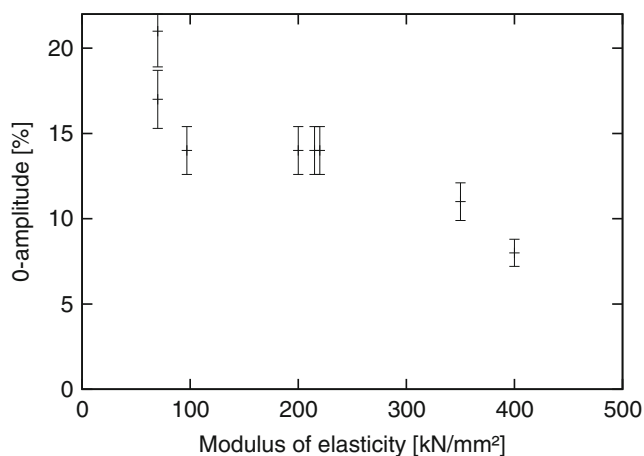
Fig. 6 0-amplitude versus runner material. There is a clear tendency, that runners made of material with higher modulus of elasticity have decreased 0-amplitude. The error bars indicate that there is uncertainty not only of the 0-amplitude measurement, but also of the modulus of elasticity

Fig. 7 0-amplitude versus control signal's slewrate for forward (*positive*) and backward (*negative*) direction, measured with **a** the method presented in [33] (*intersection*) and **b** measured directly, identifying the smallest significant step size. Both methods show a similar progress with a 0-amplitude's minimum for moderate slewrates. Though intersection method delivers larger 0-amplitude values

with characteristic depth and width. It could be thinkable that the amplitude of the actuator has to overcome this imprint to generate persistent steps. Therefore, the width could be a quantity similar to z_{ba}. With rising stiffness, depth and width of the imprint decrease and so does 0-amplitude. Calculations indicate that the value of the imprint's width is not in the range of z_{ba} but rather two orders of magnitude higher. However, the question comes up if the imprint moves along with the element, how the element can overcome the critical distance. An unambiguous explanation is not found yet. Nevertheless, measurements indicate that proper choice of Youngs modulus can bisect 0-amplitude and this indicates that the material-conditioned part of the 0-amplitude is comparatively large. If the run in Fig. 5 is extrapolated to unlimited Youngs modulus, 0-amplitude will likely run asymptotically to the value which is caused by the other (constant) 0-amplitude causations. It has to be stated that Fig. 6 can only show a tendency. In reality, every single material has it's own properties. Two examples of materials which sometimes do not follow the discussed laws are glass and a special stainless steel (1.4301). In addition, this even more complicates measurements with exactly defined parameters.

4.1.3 Influence of the slip's slewrate in the control signal

The second investigated effect is the influence of slewrate (the slope during the slip phase). In [33] it was investigated using an indirect method where it is calculated from several measured step lengths. The result

using this method is shown in Fig. 7, "intersection". Because of several uncertainties in the method, a second method is introduced. It is based on selecting an amplitude with significantly measurable step size, and decreasing amplitude until step size cannot be separated from noise. In Fig. 7 it is named "direct". It can be concluded, that the runs of both methods vary in quantity, but qualitatively show the same trend. A minimal 0-amplitude can be identified for moderate slewrate. Furthermore, 0-amplitude indeed is influenced by control signal, namely the slewrate. Finally, effect of slewrate on 0-amplitude is weaker than that of runner's Youngs modulus, but it can be detected.

Of course these two measurements can only cover a small area of the cumulation of effects on 0-amplitude. But, it is assured that z_{ba} can not be a constant for the preconditions presented here. Therefore, at least z_{ba} has to be modeled with dependence on material, preload and slewrate as a minimum for exact model response. The fact that material has large influence on slewrate indicates that 0-amplitude is mainly an issue of surface mechanics and therefore friction. Another interesting point is that the slewrate changes the asperities response. This points to material properties which are dependent on the rate of deformation [56]. This is a comparatively young area of material research. An integration of such characteristic into the model in the near future is unlikely. Other possible causations such as the influence of elastic joints (e.g. glue) or parameters of the piezoactuator can not be characterized easily. It can be deduced that these can be summed

74

J. Micro-Nano Mech. (2011) 6:65–87

up to a persistent, but comparatively small part of the 0-amplitude.

4.1.4 Youngs modulus and hardness

Let us again discuss the dependency of runner's material on 0-amplitude. We have chosen Youngs modulus as a criterion to evaluate the material. From the contact mechanic's point of view, hardness is a parameter also strongly connected with surface mechanics. Hardness can be defined as the resistance of a material against indentation [57]. Generally, there is no correlation between Youngs modulus and hardness, because hardness is associated with plastic deformation and Youngs modulus with elastic compliance. Additionally, Popov derived the correlation that hardness equals to three-times tensile strength [35]. In tensile tests the elastic and plastic limits are determined. If z_{ba} would correlate to elastic and z_{ss} to plastic deformation value, both parameters could be calculated out of material-related constants. Indeed this is the same approach as that of Popov. In mechanical engineering sciences hardness and Youngs modulus are considered discretely (If a mechanical part is hardened, it's Youngs modulus remains widely unchanged). For the sketched conditions the impression is created that Youngs modulus and hardness correlate to each other, because the arrangement of the materials sorted by (calculated) hardness leads to a similar trend. A formula characterizing the state of deformation was presented, where the index of plasticity is calculated [58]. This index decides whether the asperities can be characterized as elastic or plastic or both. Interestingly the hardness of the surface and the combined Youngs modulus are part of the calculations (and the hardness is expressed as a pressure). What remains are the questions what the mechanisms behind these developings are, and which properties make a material suitable for application with e.g. low 0-amplitude? Large Youngs' modulus, hardness or other properties? We also tried to find criteria to separate materials, e.g. by the orientation of gliding planes or their microscopic structure (e.g. crystalline, amorphous, face centered). But this approaches did not come to a result. Either much more measurements with slightly differing material properties have to be done and analyzed or new ideas from material theory have to be developed. Again, it turns out to be a problem of empiricism or theory.

4.1.5 Transition between elastic and plastic deformation

Another problem is the transition from the real contact with many asperities to the single "standard" asperity

in the simulation model. Friction is a phenomenon with statistical behavior, two measurements rarely turn out to be the same. At the moment it seems that model-given generalization is valid. If model accuracy rises in the future, this will have been kept in mind.

As already mentioned, the index of plasticity itself could be used to determine if the asperities act elastically or not. It could be done in such a way that the mentioned function replaces the $\alpha_{\text{transition}}()$-function in an adequate manner. Though this approach is not followed up in this paper. The index of plasticity also depends on the average value of the asperity's height gradient. In contact theory it is derived that this value is dependent on scale. That consequently leads to different deformation curves with different scales. But, this effect could not be affirmed. In fact a minimum surface roughness for proper function of the runner of the stick-slip drives was observed. If surface quality was enhanced, no significant effect on 0-amplitude was detected. Popov points out that surfaces with fine finish turn out to deform more elastic [35]. The effects could not be confirmed with our setup.

4.1.6 Phases in which 0-amplitude occurs

The effect of 0-amplitude can also be discussed in terms of time-dependent occurrence with respect to the control signal. Figure 1 shows a seven-phase model of the stick-slip positioning process. Phase 0 describes the initial rest position without movement. Therefore the asperities are not bent in a distinctive direction. Due to the slow forward movement of the sliding surface, the asperities begin to bend. This does not induce a significant movement of the runner (presliding 1–phase 1 in Fig. 2). The bending of the asperities without resulting motion is called presliding. The subsequent movement of the sliding surface causes an extensive bending of the asperities and finally a simultaneous movement of runner and sliding surface (phase 2–stick). Phase 3 describes the point of reverse. It is reached because of the slowdown of the sliding surface movement. In this point the asperities unbend for a short time until the fast backward movement starts. Again a bending of the asperities in the opposite direction starts ("slowdown 1" and "presliding 2" or phase 3 and 4 in Fig. 2). The adjacent fast backward movement causes the slipping between sliding surface and runner ("slip", phase 5). The end of the slip is initiated by the slowdown of the fast backward movement ("slowdown 2", phase 6), which finally results in rest condition due to damping effects. On the basis of this seven-phase model it can be assumed that the two presliding phases comprise the 0-amplitude. This

conclusion can be understood by the following theoretical procedure: By reducing the step size—caused by reduction of the control signal's amplitude—to the point of "no stick and slip generation", just the bending of the asperities in the presliding phase remains. The transitions between the different states are essential for understanding the 0-amplitude, which is the limit of this oscillating movement. The stick phase can be treated as a quasi static state, if vibrations are fully damped. What remains are conditions with clear changing asperity deflection z (such as "presliding 2", "slip" and "slowdown 2"). Therefore, the transitions from and to the slip phase come into the focus. A simple formula can help to describe the general coherency

$$s_{measured} = s_{exitation} - s_{backstep} - s_{0-amp.},\qquad(9)$$

where s stands for a step component and $s_{exitation}$ means the amplitude of the actuator. For example, an excitation of 160 nm with backstep and 0-amplitude of 30 nm would result in a step length of 90 nm (In some publications, step length is also called net displacement [59]). If we apply this formula on our measurements we found that not every material follows this law, e.g. tungsten. With a low 0-amplitude and very low backstep the runner should exhibit a step size slightly below the maximum step size. However, step size for tungsten is almost identical to other materials. Obviously, there must be a "hidden" 0-amplitude under distinct circumstances.

4.1.7 How to face 0-amplitude

It was stated that transition progress also influences 0-amplitude (and the shown dependence on slewrate is a proof). Several ideas exist to influence the state of asperities for different purposes. In the following subsection such ideas will be discussed. The "state" of the asperities can also be expressed in terms of dissipative (plastic) and non-dissipative, potentially recoverable parts. Most likely the latter will be the elastic deformations. As far as the LGM does not differentiate between pure elastic and plastic deformation, modeling of methods making use of "recoverable deformation" only makes sense with the EPM. According to the definitions in [40], z is the elastic, recoverable part of the deformation and w the plastic, dissipative part.

Finally there is the idea, if an effect of 0-amplitude is possible without pure elastic deformation trend. An example could be a forward step where elastic and plastic parts are present, followed by a (smaller) step also with both types of deformation. The result could be similar to the effect of 0-amplitude. Another case could be a sawtooth excitation signal with symmetric shape, which is indeed a triangle signal. This normally corresponds with very high stick-slip frequencies. Then it can happen that the stick more and more becomes slip, and finally two slip phases with inverted sign result at most in a vibration of the runner. But our definition of a stick-slip cycle is abandoned under such conditions. Hence, it is difficult to create conditions where mixed deformation leads to effect of 0-amplitude.

It can be concluded that material has one of the main parts on level of 0-amplitude. Other effects can be seen, but either gathering reliable data or derivation of effects from theory is difficult. In the following subsection it is outlined that there is likely a recoverable part of the 0-amplitude which can be specifically influenced.

4.2 Aspects of elastic deformation

In the former section is was stated that there are elastic deformation parts. In the EPM, elastic part is the main cause for vibrations shown in Fig. 2. This elastic deformation is unavoidable, it is always initiated by the slip impulse. This is a great difference to the simple treatment of stick-slip devices just exhibiting two phases. In practice, there are several ideas how to face elastic deformation:

– Disable vibrations by adding a secondary impulse to the slip (input shaping, presented in [59]),
– Recover the elastic deformation and utilize it for increased step size (unpublished method by members of the authors' division),
– Minimize elastic part by e.g. selecting an adequate material combination (idea by the authors).

Input shaping is a technique to transfer a given control signal into several discrete steps to avoid vibrations [60, 61]. The group around Breguet used it to eliminate the vibrations occurring after the slip in a mobile micro robot. The vibrations are similar to that in this paper. However, the dynamic range in [59] is lower because the complete robot (with different actuators) is part of investigation. The resulting technique is to subdivide the slip phase into two parts with mottled control voltage and a certain time latency. Thus, the slip signal decreases very fast to half the full value, it is hold some time and finally the slip is completed. It is shown that the method increases repeatability and improves velocity response of the robot. From this paper's point of view, input shaping is a method to eliminate elastic deformation by adding "negative" elastic deformation. In other words, it is tried to set the asperity's average deflection to zero at the end of the slip. Hence, the

76

J. Micro-Nano Mech. (2011) 6:65–87

system is at rest at the end of the slip and vibrations do not occur.

Another idea was investigated by the group of the authors of this paper: Performing clearly increased step sizes by adding hold times to the control signal. In a way it is similar to the method of input shaping, but moreover the aim is to recover the elastic deformation in contrast to eliminate it. Preliminary investigations are based on holding times before and after the slip, which lead to approximately 50% increased step size (180 nm instead of 130 nm) at distinct conditions. Admittedly this works only with comparatively high control velocities above 10 kHz. Furthermore the runner has already to be at high velocity (and therefore had to be accelerated with "usual" control shapes, which makes technical implementation difficult). We tried to adjust the effect with the EPM, and the increased step size could be detected. At the moment there is a lack of authentic data and therefore the matter will still be investigated.

The third addressed way of handling elastic deformation sounds trivial: Selection of a fortunate material combination. This can be an alternative instead of changing the control signal. We observed this possibility during measurements: For gliding surfaces made of tungsten, virtually no vibration was observed (see Fig. 8). At the same time, the backstep was extremely low. It was already stated that step size for tungsten is almost the same as for other materials anyway. In terms of elastic deformation, we have to conclude that either the elastic vibration potential is very low due to unknown material properties (maybe very high damping) or we did not detect the vibrations properly. Another explanation could be the high Youngs modulus which

Fig. 8 Two different step developings: material combinations tungsten and aluminum each with ruby, mechanical preload 1 N. Tungsten shows small backstep and virtually no vibrations

leads to small z_{ba} and therefore to low elastic deformation potential.

4.3 Blocking preload

In previous sections the friction progress on the basis of surface asperities was discussed. A very important parameter for stick-slip devices is the normal contact force, further called preload. It is documented that stick-slip performance strongly depends on the proper choice of preload. If preload is too low, the runner can not be transported, in the opposite case, slip can not be established and the runner just oscillates. Thus, this are two cases which limit the function of a drive, but in between there is a range with continuous stick-slip function. Naturally stick-slip parameters vary, e.g. step size decreases with rising preload. The modeling of this coherency will be shown in Section 5. Having the relevant literature in mind, it can be stated that preload was not intensively investigated yet. An example of the effect of preload can be found in Fig. 5. Step size is above 100 nm for low preload and decreases linearly with rising preload. With preload of approximately 5 N step size becomes zero, plastic sliding can not be established (and further on likely no elastic deformation). From the point of view of maximum step size low preload is beneficial. It will be shown later that larger preload is better in terms of generating forces. Thus, it is unknown how to systematically optimize a device for given design specifications.

It seems to be evident that low preload leads to an asperity-defined friction trend. At the same time, high preload tends to solid body contact and therefore solid body theories such as e.g. Hertzian contact theory could come to the fore. Now, the transition between both states is unexplained. Starting at low preload and increasing, the asperities likely will be pressed on each other and therefore change their parameters. In contact theory there exist individual formulas to estimate e.g. the real area of contact, the number of asperities in contact or the their limit of plastic deformation [35]. Though these approaches are far away from practice from our point of view. Figure 9 shows to what extend the point of zero step in Fig. 5 depends on the choice of the runner's material. There is a clear tendency that stiffer materials allow a step generation at higher preload. In terms of the EPM this can not be modeled, on the one hand because preload trend is not covered (compare Fig. 5) and on the other hand it is not known how to integrate material data into the model parameters. The next section will deal with this problem. An alternative explanation could again be found in Hertzian contact theory. If the actuator
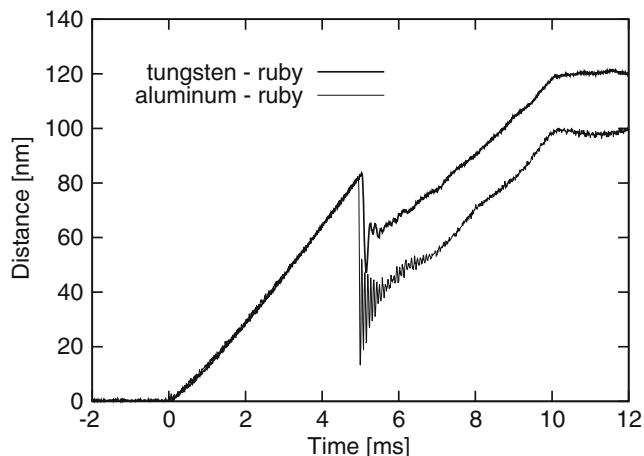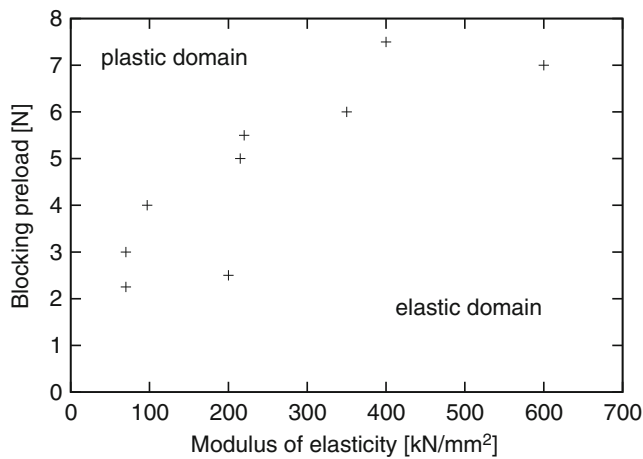
Fig. 9 Rising blocking preload with increasing runner material's modulus of elasticity. There is a proportional tendency. The points coarsely mark the transition from elastic to plastic progress

Fig. 10 Values of σ_0 theoretically derived. Note the logarithmic scale for σ_0. An estimation for actual measurements is right between the two theoretic approaches from Breguet and Popov. However, quantitative values differ for some orders of magnitude

is able to generate a certain, constant displacement, and if higher Youngs modulus causes a more narrow indentation, an actuator could more easily overcome this indentation and generate steps.

Probably the value of tangential compliance will increase with rising preload if one has the image of compressed, shortened asperities (with less compliance) in mind. Simulations and mathematical considerations show that the vibration frequency is defined by σ_0. In measurements a dependency between preload and vibration frequency could not be identified without a doubt.
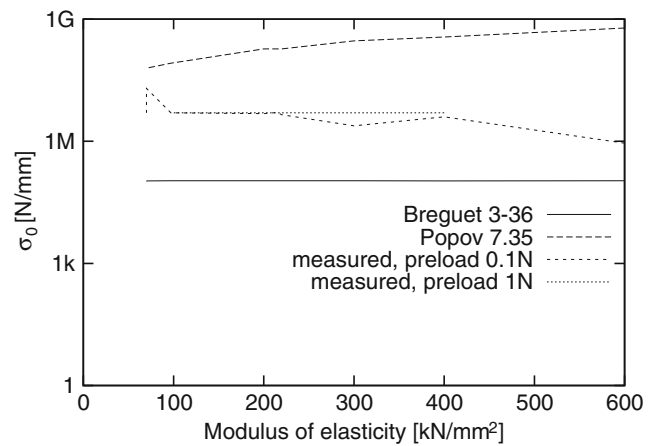
4.4 Theoretical derivation of model parameters σ_0, σ_1 and σ_2

This section deals with theoretic derivation of parameters σ_0, σ_1 and σ_2 introduced with Eq. 1. It was denoted that friction force is strongly connected with surface mechanics. Furthermore, the parameters describe model progress in terms of compliance, damping and lubrication influence for the lumped model's asperity. Hence, parameter's derivation from material and surface conditions suggests itself. Though this is a difficult approach.

4.4.1 Treatment of σ_0

From the point of view of material science σ_0 represents the material's Youngs modulus. In surface mechanics it is the tangential compliance. Several theoretical derivations for σ_0 exist. Unfortunately, values strongly vary and thus selection of proper values is complicated. Figure 10 shows the bandwidth of two theoretical and

two semi-experimental approaches to identify σ_0. In [27], Eq. 3–36, a derivation of tangential compliance is presented, which goes back to [62]. It depends on Youngs modulus and Poisson's number and on geometric radius of the circle-shaped contact ("Breguet 3–36" in Fig. 10). Although Youngs modulus changes, derivation delivers almost constant value for σ_0. Another trend is shown ("Popov 7.35"). This approximation depends on shear modulus, number of asperities and Poisson's number. In contrast to Breguet's developing, it is explicitly increasing with value of Youngs modulus (note the logarithmic scale of σ_0). Generally, approaches of Breguet and Popov differ with three orders of magnitude. A possible explanation could be the fact, that some values needed for calculation are unknown for the present material and have to be estimated or calculated from other values. An example is the shear modulus. Despite the uncertainty of material data, it seems that theory can deliver only qualitative numbers for σ_0.

Another semi-experimental approach is introduced by the authors. It consists of the measurement of single steps such as in Fig. 8 and adjacent determination of vibration frequency for different runner materials. After that, it is assumed that runner's mass and surface asperities build mass-spring system following

$$\omega = \sqrt{\frac{c}{m}}, \tag{10}$$

which can be used to describe asperity-originated vibration frequency

$$c_{\text{surface}} = \sigma_0 = 4\pi^2 \cdot m_{\text{runner}} \cdot f_{\text{vibration}}^2. \tag{11}$$

78

J. Micro-Nano Mech. (2011) 6:65–87

Finally, calculated values for two different preload settings are shown in Fig. 10. Basically the values are inside the bandwidth defined by Breguet and Popov, although the approach is very simple and relies on measurements. Preload of 1 N leads to almost constant values similar to Breguet, preload of 0.1 N shows an anti-proportional tendency to Youngs modulus. There is no correlation to theoretically derived values.

It has to be concluded that theoretic derivation is not able to identify values for σ_0 without ambiguity. Even though an interval of probable values can be defined, calculations depend on material constant which cannot be clearly identified. The measurement results of the authors indicate that very simple approaches lead to comparable results.

Another interesting fact is implicitly available, the dependency of σ_0 on preload. For calculations of Breguet, preload is comprised in geometric radius of the circle-shaped contact. This leads to weak effect of preload with cubic root. On the other hand, Popov's equation does not include preload, neither directly nor indirectly. From theory's point of view, it is unknown how to handle increasing preload and friction transition in terms of surface compliance.

In the EPM, on the one hand σ_0 defines the vibration frequency. On the other hand σ_0 also assesses maximum deflection of asperities z_{ss}. The advantage is the straightforward number of parameters. But, as will be shown in Section 5, it can be reasonable to separate into two independent instances $\sigma_{0,ss}$ and σ_0^* to reproduce empirical results. This matter is unhandeled in terms of theory yet. As already mentioned, σ_0 is also linked with the forces a stick-slip drive can generate in simulation. More on that in Section 4.6.

4.4.2 Treatment of σ_1

In EPM, σ_1 mathematically represents attenuation coefficient of the vibration frequency. In reality, damping of the vibration likely is influenced by several, unknown parameters. We propose to determine σ_1 empirically. But we did not specially investigate this parameter. A coherency between σ_1 and rate-dependent elastic progress or configuration of gliding planes is highly speculative. Some data indicate that material damping could be linked up with face-centered property, sometimes results contradict each other. Though, the authors were not able to proof this statement.

4.4.3 Treatment of σ_2

In both LGM and EPM, a friction force caused by lubricants (viscous friction) is considered (compare Eq. 1,

σ_2-term). In Section 5.1 it is stated that differential velocities are low (far below 1 ms^{-1}). In addition the use of lubricants in stick-slip micro drives is avoided. This is caused on the one hand by keeping the vacuum environment clean, on the other hand by the wish to establish greater stiction. Breguet draws the conclusion that viscous friction is of less importance, this is in accordance to other authors. In [63] it is stated that viscous friction can be neglected for small relative velocities in systems with dominant presliding developing. Indeed this is the case here. Thus, we can neglect σ_2 for simulation of stick-slip micro devices.

4.5 Properties of piezoelectric actuators

A very important aspect of stick-slip micro devices was under-represented in this paper yet: The widespread use of piezo-ceramics as voltage-deformation converters. Piezoceramics (PZT 5H or PIC151, [64]) used here offer several beneficial properties:
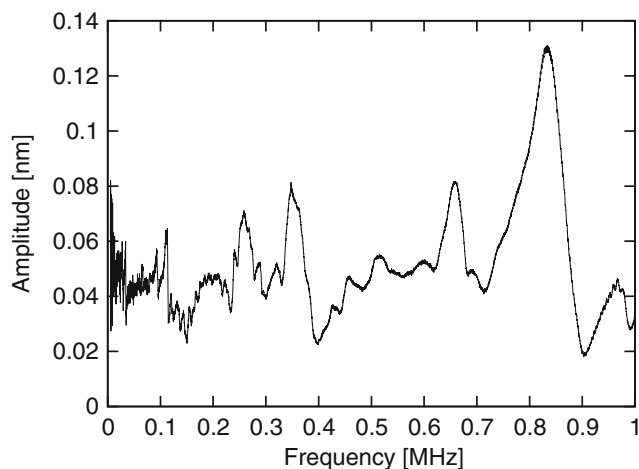
–   Their high dynamic range,
–   a high resolution in terms of small possible stick-slip step lengths,
–   the great potential for miniaturization and
–   a large mechanical stiffness or low compliance, respectively, which is important for optimal response of systems with small accelerated masses.

Nevertheless also piezo-ceramics have drawbacks: The nonlinearities caused by **piezo-hysteresis** and the extensive fabrication [39]. It was mentioned several times in this paper that the piezoactuator is likely the reason for nonlinear trend as in Fig. 2. This assumption is supported by the fact that sometimes step length depends on the preliminary step's direction. At this point it is unclear how piezo-based hysteresis influences performance of stick-slip process. There are mainly two reasons why the authors preferred an ideal, linear voltage-deflection converter instead of a piezo model yet: The complexity of modeling a piezoactuator on the one hand (see [65, 66] for hysteresis modeling), and the fact that influence of piezohysteresis appears to be limited on the other hand. As far as the authors experience is concerned, piezo hysteresis influences step shape (nonlinear run and second stick has less deflection), but fewer step length. Furthermore, outlined investigations showed that material has by far the most influence on e.g. 0-amplitude. So, until now there was less occasion to have a focus on piezo hysteresis. With increasing prediction quality and improved understanding of the coherencies, piezo hysteresis could become of interest in the future.

An important fact was prepared in [34], but will be repeated here: The force limit of our piezo actuators in the meaning of this publication (actuation with zero deflection) plays not a role in terms of blocking preload (compare Fig. 5). In the publication it was shown that preload is in the range of several *N*, whereas piezo's force limit is in the range of *several decades of N*. Therefore, blocking preload is a phenomenon caused by surface mechanics exclusively, not by piezo properties.

As already mentioned, a linear ratio between control voltage and actuator deflection was assumed yet. The high effort of modeling piezo properties is in contrast to presumably moderate gain in knowledge. Maybe influence on 0-amplitude or σ_0 can be judged better.

In this paper we concentrate on systems with very stiff actuators, so that mechanical compliance of the actuators can be neglected and modeling of "infinitively stiff" actuators is arguable. To justify this, compliance should be measured. Especially for piezoceramics this is a complicated matter, however, measurement of the actuators eigenfrequencies can be done with special equipment. In collaboration with another institute using a laser Doppler-interferometer (from Polytec, MSA-400) we were able to measure the response of the unloaded piezoactuators including actuator's moving parts (such as ruby hemispheres as wear-resistant material). The result can be obtained from Fig. 11. The actuator was exposed to a periodic signal and the resulting vibration amplitude was recorded. Excitation voltage and vibration amplitude are low due to measurement procedure. The first eigenfrequency can be easily identified at 820 kHz. This proves the assumption that the used piezoactuators are comparatively stiff and therefore the mechanical compliance of the piezoactuators can be neglected in our model.

4.6 Generating forces

In recent literature, main interest for modeling stick-slip micro devices was to reproduce step size and to identify important parameters. From the authors' point of view, also "forces" should be in the focus of research, namely the **generated force**, the force a stick-slip device can carry on the runner. In other words, the question could be: Which load can a stick-slip axis lift (in terms of robotics) and what are the important parameters? In [34] the general process of generating stick-slip-caused forces is investigated. It is also shown that the EPM can qualitatively reproduce the generated force. Nevertheless it is stated that force levels are low compared to measurements and that influence of preload is not reproduced properly (In Section 5.3 an empirical approach to face these lacks is shown). Early simulations showed that value of σ_0 in EPM determines the level of generated force. It seems that surface compliance depends on level of control amplitude in a nonlinear way. However, this coherency can not be covered by the EPM yet. The idea is supported by a measurement in which several runner materials and the accordant generated force were measured with different preload (Fig. 12). All shown characteristics show a rising shape with clear maximum and decrease for high preload. Furthermore materials with higher Youngs modulus clearly show larger generated forces combined with larger preload. It is clear that material properties in terms of force generation can only be
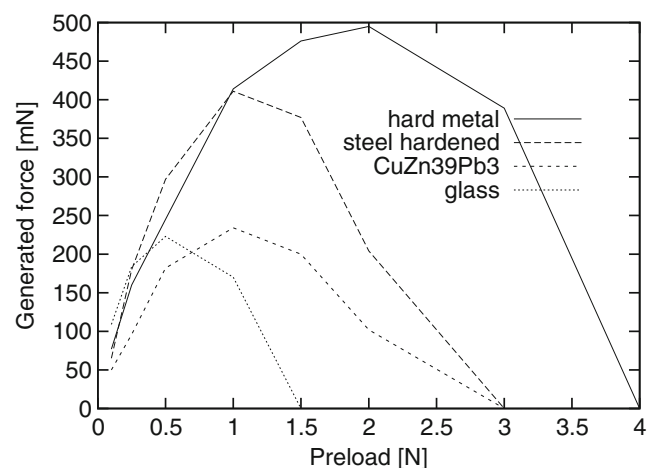

Fig. 11 Vibration amplitude over excitation frequency for a piezoactuator used in this paper. The first eigenfrequency can be easily identified at 820 kHz. This is in accordance to a simulated value of 975 kHz in [39]

Fig. 12 Different levels of generated force dependent on preload and runner's material

80

J. Micro-Nano Mech. (2011) 6:65–87

represented in the model by σ_0 yet. At the same time, theoretic derivation is impossible due to the already mentioned questions, in the first place: How can the transition between asperity-based friction to solid-body friction be described? Because of this reasons we will focus on empirical modeling later on.

4.7 Other aspects linked with friction

Surface roughness is often assumed to have a large influence on friction. The authors could not affirm such effect. Indeed we identified a certain minimum surface quality to get our devices to work. But, with rising surface quality, stick-slip performance remains constant. Likely the asperities have to be "short" enough to enable general slipping with a given maximum actuator deflection, which can explain the mentioned minimum surface quality. But there seems not to be a significant influence as far as stick-slip step's or model's parameters are concerned. Other investigations support the idea that roughness does not influence friction over several orders of magnitude [67]. We can conclude that a minimum surface quality is needed and that this is the only precondition for proper function. Modeling of surface roughness or quality, respectively, is superfluous.

Wear is another important aspect for stick-slip micro devices. A comprehensive work on that matter can be found in [29]. Due to the fact that the focus of this paper is on modeling basic properties, wear is not an issue yet. Before wear can be integrated into the model, methods and categories have to be introduced anyway and wear mechanisms have to be described numerically.

Due to literature research, several **special friction effects** came up:

– Changed friction due to high temperatures caused e.g. by high relative velocity [68, 69]. Due to low relative velocities and high melting points of the used materials we can drop this effect.
– Chemical and atomar forces such as adhesive and van-der-Waals forces can be neglected due to comparatively large scale of friction contacts and body dimensions.
– Charge transfer can lead to electric charging in such devices [70]. The effect is very weak and therefore can be neglected.
– Influence of ultrasonic noise on friction is matter of interest [35, 71]. Having the fact in mind that the slip phase can be compared with an impulse exciting also ultrasonic noise, this could be of importance in the future. Nevertheless at the moment there is no evidence for such effect.

It can be concluded that friction in terms of stick-slip micro devices is a manifold matter. After review of several effects, the CEIM model will be established.

5 The CEIM model: adaptation of the Elastoplastic model

This section documents adaptations of the EPM. Most of them raised empirically because the underlying friction theory is not understood yet. The adaptations are introduced to gather an improved prediction quality.

5.1 Evaluation of kinetic and static friction coefficient

Investigations of Breguet showed that static friction has less influence on the stick-slip response of a micro actuator in contrast to dynamic friction (see Section 2.2). However, results are mainly supplied by simulations. For that reason measurements should proof the simulation. One of the parameters defining friction transition between sticking and sliding is the range of differential velocity v_{diff}. Simple calculations and comparison with measurements of the authors generally lead to slow differential velocities between the friction pair ruby sphere and hardened steel sphere even during the slip (<200 mm/s). Unfortunately there is a lack of reliable literature values for such material combination, low velocities and distinct surface conditions (virtually no lubricant, high surface quality). Hence, the coefficient of friction was measured with a custom-made tribometer [72]. The developing of friction coefficient (Fig. 13) is clearly independent of the selected differential
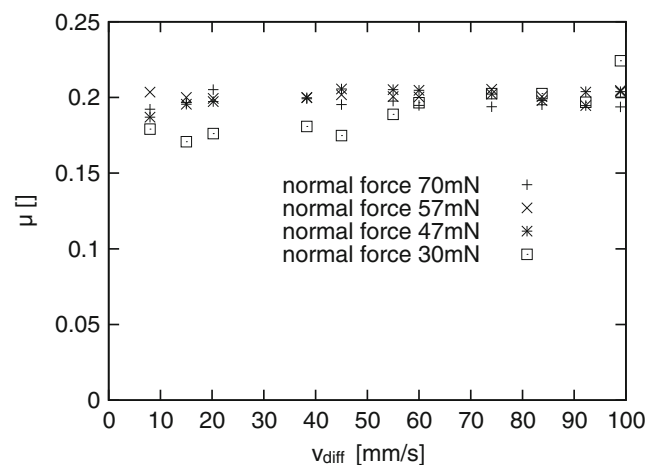
Fig. 13 Friction coefficient μ between ruby and hardened steel (both sphere surfaces, point contact) was measured for typical differential velocities. Kinetic friction remains constant (adapted from [72])

velocities and normal forces. It is a strong indicator that Stribeck curve can be neglected for the current application of the EPM. This goes along with the removal of the parameter $v_{Stribeck}$ at least, resulting in a constant kinetic friction coefficient. Results of the authors also showed, that the difference of the absolute values of $\mu_{kinetic}$ and μ_{static} does not influence simulation results significantly. For this reason we propose not to distinguish between the two coefficients, but to use simply one single coefficient μ_{CEIM}. This reduces the number of model parameters. It can be concluded that Stribeck curve has no importance for stick-slip micro drives (which was expected for dry friction conditions). This could be interpreted in such a way that a drive only needs the states "sticking" with $v_{diff} = 0$ and "slipping" with $v_{diff} = v_{slip}$. This means, the transition band between the two velocities, which is passed through very fast, is of no meaning in terms of Stribeck's friction (this does not apply for 0-amplitude).

This "review" of Stribeck' and Coulomb' friction effects can be enhanced. In Section 5.6 we will discuss an even more consequent idea to handle the evanescent meaning of μ for stick-slip micro drives.

5.2 Modeling of the mechanical design

In the EPM presented in Section 3 dynamic of surface mechanics is reduced to a single, lumped asperity and the "global" mechanical conditions are represented by only two parameters: The runner's mass and the level of preload. The lumped asperity indicates that in the EPM there is only one single frictional contact. Indeed this is in contrast to real stick-slip devices, where either a guiding generates additional dynamic (frictional) forces or the guiding also functions as actuator at the cost of multiple contacts afflicted with stick-slip friction. Therefore, the model generally has to be adapted, either by adding guiding characteristics or by modeling each friction contact with individual parameters. However, the latter will dramatically increase calculation times and, even more important, individual friction values are unknown.

Breguet configured the mechanical model for his simulation in such a way, that there is only one stick-slip contact. But his prototypes exhibit at least five point contacts for determinateness. Same applies for similar modeling approaches. Driesen proposed an n-times higher value for σ_0, with n as the number of stick-slip contacts [19]. It can be concluded that impact of mechanical constraints was neglected, likely because complexity dramatically rises and meaningful parameters are unknown.

The authors of this paper decided to denominate **preload** as the **sum of single normal forces** in the simulation. Indeed, this is an almost arbitrary choice because of uncertain data. But, consistency with measurements is not bad. In Appendix the derivation of six forces holding a runner dependent on preload is presented. Preload in this sense means the force which can be measured practically using a load cell. To gather a comprehensive approach, several simplifications have to be made. Due to geometric constraints the effective sum of single normal forces is more than two times higher than measured preload. With respect to simplifications, it is difficult to reason regularity. All simulation results in this paper were specified with the measured values (as if there was a single asperity with the measured level of preload).

Popov points out that several simplifications for simulation of a friction model are permissible [35]:

- Deformations can be treated as static if their velocity is far below velocity of sound.
- The potential energy and thus the conditions of forces and their displacements are local phenomena. They depend on the configuration of the (micro-) asperities, but not on the macro body properties such as dimensions and shape.
- The kinetic energy is a global property, which depends on the macro-configuration of the bodies, but not on the micro-asperity conditions.
- Many three-dimensional continua can be expressed using one-dimensional systems.

These conditions doubtless apply for the present problem. Nevertheless there is the question, to what extend these assumptions quantitatively influence simulation results.

5.3 Empirical modeling of preload characteristic

As indicated with Fig. 4 in Section 3, $z_{ba} - z_{ss}$ ratio defines the amplitude-progress. A ratio of 50% is identified to represent measured proportions well. The value of z_{ba} then decides at which level of preload the step length decreases to zero. At the same time, 0-amplitude increases with preload, and preload-dependency cannot be covered yet (compare measurement in Fig. 5). For that reason we propose to define

$$z_{ss} = 2 \cdot z_{ba}, \tag{12}$$

and set z_{ba} dependent on preload in such a way, that 0-amplitude increases with preload,

$$z_{ba} = m \cdot f_{preload} + n. \tag{13}$$

82

J. Micro-Nano Mech. (2011) 6:65–87

For preload of 1 N, $m = 2 \cdot 10^{-8}$ mN^{-1} and $n = 1 \cdot 10^{-8}$ mN^{-1} this will result in $z_{ba} = 30$ nm and $z_{ss} = 60$ nm, which represent realistic values compared to the actuator displacement of 160 nm in Table 1. Values for linearization are a first result of empirical measurements. With a broader data basis, better modeling with higher order is advisable. The simulation result is shown in Fig. 14. An alternative attempt to influence 0-amplitude via σ_0 was not sucessful. It can be concluded that above modeling of z_{ba} is a very easy, but effective approach, although it is bases only on empirical data. Concretely, z_{ba} simply increases with preload, which results in larger breakaway distance and shorter step lengths. In other words, preload defines z_{ba} and therefore 0-amplitude.
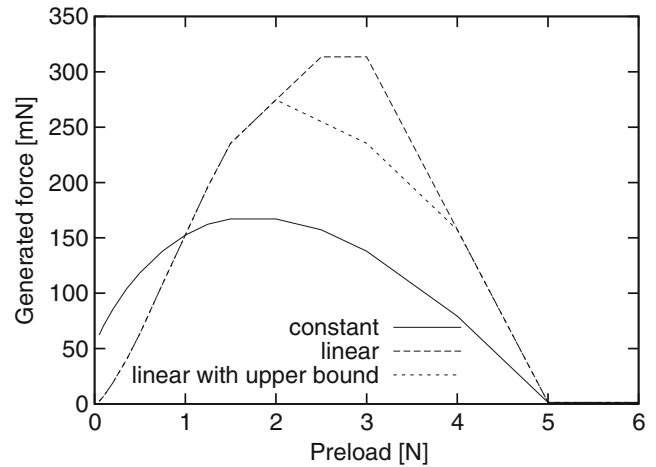
Interestingly, value of z_{ss} has virtually no meaning for stick-slip progress. Absolute value does not influence simulation results. But in terms of $z_{ba} - z_{ss}$ ratio, it has to be greater than z_{ba}. For comparison only: In [41], a ratio of 70% was proposed.

5.4 Empirical modeling of force-generation method

In [34] stick-slip micro devices are used to generate arbitrary, quasistatic forces mainly dependent on control amplitude and preload (see also Section 4.6). Modeling of this method was only accomplished insofar to show that the EPM can qualitatively render it. Several times in this paper it was mentioned that σ_0 defines level of generated force in the simulation model. For the original EPM, σ_0 is a constant value. This results in the curve shown in Fig. 15, "constant". Qualitative trait including a clear maximum for moderate preload is covered, even though the level of generated force is too
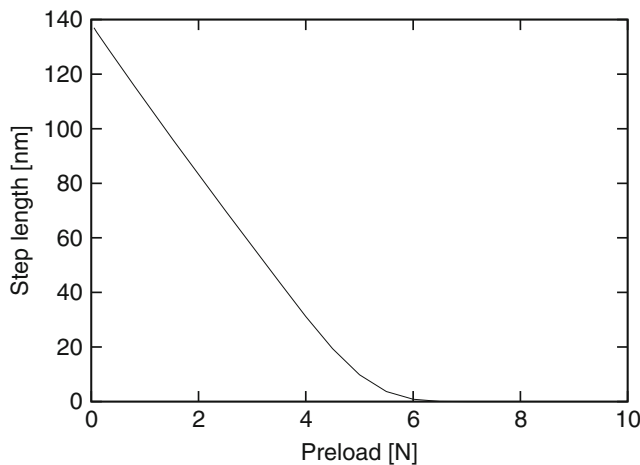
Fig. 15 Different simulated trends of generated force. With constant σ_0^* generated force has a clear maximum, but force level is low. With linear dependence on preload force levels rise but *curve* changes. An upper bound for σ_0^* leads to a force gain around the bound's according preload

low. In this section a simple correlation between σ_0 and preload is introduced with Eq. 14.

$$\sigma_0^* = o \cdot f_{\text{preload}} + p. \tag{14}$$

The equation represents an increasing stiffness σ_0^* with rising preload ($o = 5 \cdot 10^6$ m^{-1}, $p = 7 \cdot 10^6$ Nm^{-1}). This could be understood as shorter asperities or as an increased number of interconnecting asperities, respectively, resulting in increased Youngs modulus. This again leads to higher level of preload. The linear dependency generates a run such as "linear" in Fig. 15. The level of generated force is doubled, and the maximum shifts from 1.7 N to 2.8 N. To further modify the trend, the maximum value of σ_0^* was limited to the value belonging to preload of 2 N ("linear with upper bound"). Finally, the course resembles that of real measurements. Similar to modeling of z_{ba}, an adaptation to measured conditions could be performed. Again, the question remains how to theoretically derive such coherency.

5.5 The CEIM model based on the Elastoplastic model

After detailed discussion of different friction phenomena in Section 4, the modified CEIM-model (representing the authors abbreviations) is presented. As shown in Section 4.4 the term including σ_2 can be removed, also Stribeck-curve and Coulomb following Section 5.1. In Section 5.3 a new formula for z_{ba} and in Section 5.4 an improved coherency for σ_0^* were derived. Therefore, the basic Eqs. 1 and 7 can be rewritten as

$$F_{\text{friction}} = \sigma_0^* \cdot z + \sigma_1 \cdot \dot{z} \tag{15}$$

Fig. 14 Step length versus preload with linear dependency of z_{ba} to preload. Progress is the same as measured one in Fig. 5

and

$$\dot{z} = v_{\text{diff}} - \frac{\alpha_{\text{transition}}() \cdot |v_{\text{diff}}| \cdot \sigma_{0,\text{ss}}}{f_{\text{preload}} \cdot \mu_{\text{CEIM}}} \cdot z. \tag{16}$$

The four Eqs. 13–16 represent the current knowledge of the authors to quantitatively model stick-slip micro devices. Note that the parameter σ_0 was split into a preload-dependend part σ_0^* and a static component $\sigma_{0,\text{ss}}$.

5.6 Straightforward model without "classical" friction coefficient μ

If one studies the aforementioned friction model, it can be seen that μ_{CEIM} on the one hand is constant, and on the other hand its impact is reduced to a numerical constant. Main friction characteristic is comprehended in parameters such as z_{ba} and σ_0. Therefore, removal of μ_{CEIM} would be a consequent way of development.

Indeed friction "coefficient" μ can be derived using other friction- or material-related values. A good example can be found in [73], where μ is derived from shear- and surface-compliance. The approach is refined in [35] including the real contact areas and force ratios. It can be concluded that μ is not a specific value such as Youngs modulus, but it is derived from such values and therefore could be replaced.

If one considers Eq. 16, removal of μ_{CEIM} changes $\dot{z}$. However, the lack of the factor 0.2 can be easily compensated by other values in the term, e.g. $\sigma_{0,\text{ss}}$. Finally, the essential friction progress would be covered by the differential-equation character of the friction model and the dependency of parameters to external factors such as preload.

6 Conclusion and outlook

In this paper, parameters which define friction of stick-slip micro drives are discussed and a friction model for such devices based on the Elastoplastic model is proposed. The main focus lies on the minimum actuation amplitude to achieve stick-slip steps, namely the 0-amplitude. After an introduction to stick-slip micro devices and before friction-related effects are discussed, the state of research in terms of the LuGre- and the Elastoplastic-model is presented in detail. It is outlined that 0-amplitude is mainly a friction-related phenomenon and that the capability of the Elastoplastic-model to express pure elastic deformation is an adequate resource to model it. Furthermore, ability of the presented CEIM friction-model to cover effect of force generation quantitatively is analyzed. The accurateness

is documented by numerous measurements and simulation runs, but friction theory is a large area of research and several questions could not be answered yet. Although the available model is mainly based on empiricism and could definitely serve as a tool for engineers, it was unable to build a comprehensive, solid bridge to basic friction theory without ambiguity. An example for such uncertainty is the preload-dependent calculation of breakaway-distance, which could be explained both by a shortening of asperities with increasing preload or a wider imprint due to Hertzian theory. Nevertheless, there is much potential for improvements both on the side of theory and on that of practical application.

Future work can be subdivided into three parts: Theoretical work, improvement of the model (in an empirical way) and practical applications of the presented CEIM model for research. Obviously the borders are floating. A great goal still is to close the gap between theoretical ideas and practical approaches. The theoretical work will be focused on including material parameters (e.g. Youngs modulus, microscopic configuration, deformation-rate properties) to the friction model, model the piezoactuator (hysteresis) and maybe simplify the mathematical design. Furthermore, elimination of μ_{CEIM} will be investigated. Empirical development will focus on improving the accurateness of the simulated values. It will also care for friction-related effects such as wear. Another goal could be to derive equations, which describe e.g. the resulting step size dependent on all model parameters. This can result in a very fast prediction of results without time-consuming simulation runs. Obviously, theoretical and empirical development are not clearly separated, in fact it should be tried to melt them to a comprehensive conception of friction. Finally, the CEIM model can be applied to investigate effects such as step-elongation (see Section 4.2), force generation or other aspects, e.g. minimization of 0-amplitude for simplified control electronics. If 0-amplitude prooves to be the measurable equivalent to breakaway-distance z_{ba}, a testbed for optimized measurements is thinkable. Again, results could be used to gain knowledge about friction in stick-slip micro devices.

Appendix: Mechanical modeling

It was indicated that the normal force used in the EPM has to be derived with respect to the mechanical conditions of the runner. In this Appendix a first approach for the derivation will be shown. It is assumed that the runner is hold by six contacts with six normal

forces (according to reality), which cause six frictional components holding the runner in position. This is done under the terms of design for precision positioning [74]. It is assumed that the ratio between normal force and its frictional component is the same for every normal force (likely different to reality). Under this preconditions, mechanical equations for every degree of freedom can be derived. It is believed that the conditions can be transferred into a single, representative normal force value for the model. The easiest approach is to sum up all normal forces (superposition), which is done below. Figure 16a shows the runner with the twelve force components, Fig. 16b the definition of geometric conditions. The angle between the normal forces and x-direction is 45 degrees (90 degrees angle between the sliding surfaces of the runner). Three equations for force balance

$$0 = \frac{A}{\sqrt{2}} + \frac{B}{\sqrt{2}} + \frac{C}{\sqrt{2}} + \frac{D}{\sqrt{2}} - \frac{E}{\sqrt{2}} - \frac{F}{\sqrt{2}}, \tag{17}$$

$$0 = \frac{A}{\sqrt{2}} + \frac{C}{\sqrt{2}} + \frac{E}{\sqrt{2}} - \frac{B}{\sqrt{2}} - \frac{D}{\sqrt{2}} - \frac{F}{\sqrt{2}} - mg \cdot \sin(\alpha), \tag{18}$$

a)

b)

c)

Fig. 16 Sketch of the runner with forces for calculations. **a** Shows the runner with six normal forces, the six resulting frictional components with respect to the condition, that friction can only deploy in the same direction as the runner can move, namely in Z. **b** Shows geometrical conditions and **c** the runner, hold by actuator elements with mechanical preload on their part

$$0 = A_R + B_R + C_R + D_R + E_R + F_R$$
$$- m \cdot \ddot{z} - mg \cdot \cos(\alpha), \tag{19}$$

and three equations for momentum balance

$$0 = E \cdot e - F \cdot e - mg \cdot \left(\frac{a}{2} - \frac{b}{2}\right) \sin(\alpha), \tag{20}$$

$$0 = \frac{A+D}{\sqrt{2}} \cdot \frac{c}{2} - \frac{B+C}{\sqrt{2}} \cdot \frac{c}{2}$$
$$+ (F+D+B)\frac{\mu b}{2} - (A+C+E)\frac{\mu b}{2}, \tag{21}$$

and

$$0 = \frac{C+D}{\sqrt{2}} \cdot \frac{c}{2} - \frac{A+B}{\sqrt{2}} \cdot \frac{c}{2}$$
$$+ \frac{A_{\text{fric}} + B_{\text{fric}} + C_{\text{fric}} + D_{\text{fric}}}{2} \cdot a$$
$$- \frac{E_{\text{fric}} + F_{\text{fric}}}{2} \cdot a \tag{22}$$

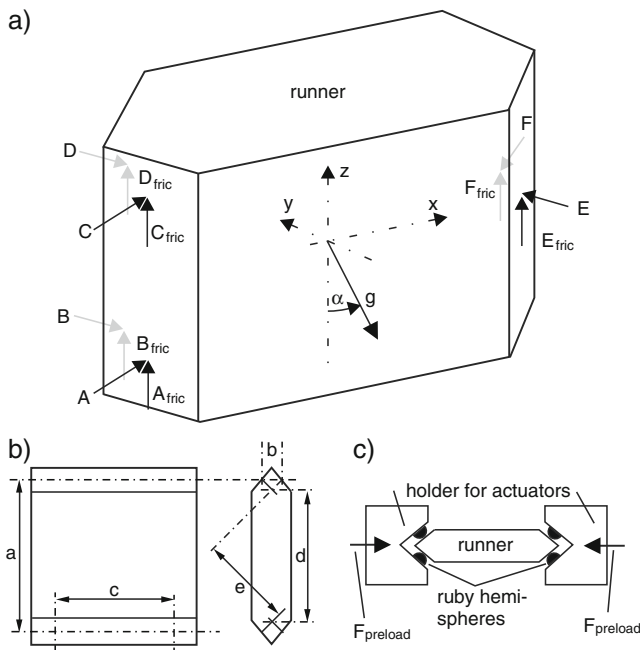can be derived. These equations can be written of the form

$$\begin{pmatrix} M_{\text{mech},11} & \cdots & M_{\text{mech},16} \\ \vdots & \ddots & \vdots \\ M_{\text{mech},61} & \cdots & M_{\text{mech},66} \end{pmatrix} \cdot \begin{pmatrix} A \\ B \\ C \\ D \\ E \\ F \end{pmatrix} = \begin{pmatrix} R_1 \\ \vdots \\ R_n \end{pmatrix} \tag{23}$$

with

$$M_{\text{mech},1}$$
$$= \begin{pmatrix} 1 & 1 & 1 & 1 & -1 & -1 \\ 1 & -1 & 1 & -1 & 1 & -1 \\ 1 & 1 & 1 & 1 & 1 & 1 \\ 0 & 0 & 0 & 0 & 1 & -1 \\ \frac{i}{2} - \frac{\mu b}{2} & -\frac{i}{2} + \frac{\mu b}{2} & \frac{i}{2} - \frac{\mu b}{2} & \frac{i}{2} + \frac{\mu b}{2} & -\frac{\mu b}{2} & +\frac{\mu b}{2} \\ -i + \mu a & -i + \mu a & i + \mu a & i + \mu a & -\mu a & -\mu a \end{pmatrix} \tag{24}$$

and

$$i = \frac{c}{\sqrt{2}} \tag{25}$$

Table 4 Mechanical parameters

Parameter	Value	Unit
a	0.015	m
b	0.002	m
c	0.005	m
d	0.013	m
e	0.007	m
g	9.81	m/s^2
$\ddot{z}$	0	m/s^2
m	0.003	kg
$f_{preload}$	0.2	N
α	90	°

and

$$R_1 = \begin{pmatrix} 0 \\ \sqrt{2}\, mg \sin(\alpha) \\ \dfrac{m}{\mu}(\ddot{z} + g\cos(\alpha)) \\ \dfrac{mg}{e}\left(\dfrac{a}{2} - \dfrac{b}{2}\right)\sin(\alpha) \\ 0 \\ 0 \end{pmatrix}. \qquad (26)$$

Figure 16c shows how the runner is hold by two actuator elements, loaded by preload. Therefore, an additional equation can be derived including preload

$$f_{preload} = \frac{E + F}{\sqrt{2}}. \qquad (27)$$

Moreover, friction coefficient μ is assumed to be equal for all six contact points. Then, the resulting friction force Q can be expressed through

$$Q = (A_{fr.} + B_{fr.} + C_{fr.} + D_{fr.} + E_{fr.} + F_{fr.}). \qquad (28)$$

Indeed this assumption must be done due to lack of individual friction conditions. Finally, Q is independent of geometry:

$$Q = \frac{m}{\mu}(\ddot{z} + g\cos(\alpha)). \qquad (29)$$

Table 5 Mechanical parameters

Parameter	Value	Unit
A	74.3	mN
B	67.1	mN
C	74.3	mN
D	67.1	mN
E	155.1	mN
F	127.8	mN
$\sum f_{A-F}$	0.566	N
$f_{preload}$	0.2	N
ratio $\dfrac{\sum f_{A-F}}{f_{preload}}$	2.8	

Therefore, row 3 in Eq. 23 can be removed and replaced by Eq. 27. This leads to a second equation system similar to Eq. 23 with degree six

$$M_{mech,2} = \begin{pmatrix} 1 & 1 & 1 & 1 & -1 & -1 \\ 1 & -1 & 1 & -1 & 1 & -1 \\ 0 & 0 & 0 & 0 & 1 & -1 \\ \dfrac{i}{2} & -\dfrac{i}{2} & -\dfrac{i}{2} & \dfrac{i}{2} & 0 & 0 \\ -\dfrac{i}{2} & -\dfrac{i}{2} & \dfrac{i}{2} & \dfrac{i}{2} & 0 & 0 \\ 0 & 0 & 0 & 0 & \dfrac{1}{\sqrt{2}} & \dfrac{1}{\sqrt{2}} \end{pmatrix} \qquad (30)$$

and

$$R_2 = \begin{pmatrix} 0 \\ \sqrt{2}\, mg \sin(\alpha) \\ \dfrac{mg}{e}\left(\dfrac{a}{2} - \dfrac{b}{2}\right)\sin(\alpha) \\ 0 \\ 0 \\ f_{preload} \end{pmatrix} \qquad (31)$$

For the conditions shown in Table 4, the values of the forces can be calculated to those in Table 5. It is shown that the sum of the normal forces is 2.8-times higher than measured preload due to geometric conditions. This is an indicator that mechanical conditions have to be deposited in the model. To keep effort low, assumptions for simplification have to be made. But it is unknown to which extend this is acceptable.

References

1. Spanner K, Koc B (2010) An overview of piezoelectric motors. In: Actuator2010, 12th international conference on new actuators, Bremen, Germany
2. Uchino K (2010) Piezoelectric actuators 2010, piezoelectric devices in the sustainable society. In: Actuator2010, 12th international conference on new actuators, Bremen, Germany
3. Smaract Gmbh (2010) Floetenstrasse 70, 26125 Oldenburg, Germany. http://www.smaract.de
4. Attocube Systems AG (2010) Königinstrasse 11a RGB, 80539 München, Germany. http://www.attocube.com
5. Klocke Nanotechnik Gmbh (2010) Pascalstr. 17, 52076 Aachen, Germany. http://www.nanomotor.de/
6. Imina Technologies LLC (2010) Ch. de la Raye 13, CH – 1024 Ecublens, Switzerland. http://www.imina.ch/
7. Xidex Corporation (2010) 8906 Wall Street, Suite 703, Austin, Texas 78754. http://www.xidex.com/Xidex/Home.html
8. Edeler C, Jasper D, Diederichs C, Fatikow S (2010) Fast and accurate pick-and-place automation with nanorobots. In: Actuator2010, 12th international conference on new actuators, Bremen, Germany

9. Zesch W, Buechi R, Codourey A, Siegwart RY (1995) Inertial drives for micro- and nanorobots: two novel mechanisms. In: Proc. SPIE

10. Munassypov R, Grossmann B, Magnussen B, Fatikow S (1996) Development and control of piezoelectric actuators for a mobile micromanipulation system. In: Actuator1996, 5th international conference on new actuators, Bremen, Germany

11. Dooley JA, Lindensmith CA, Chave RG, Fultz B, Graetz J (1998) Cryogenic magnetostrictive actuators: materials and applications. In: Actuator1998, 6th international conference on new actuators, Bremen, Germany

12. Breguet JM, Pérez R, Bergander A, Schmitt C, Clavel R, Bleuler H (2000) Piezoactuators for motion control from centimeter to nanometer. In: Proceedings of the 2000 IEEE/RS/ international conference on intelligent robots and systems

13. Martel S, Saraswat A, Hunter I (2000) Fundamentals of piezo-ceramic actuation for micrometer and sub-micrometer motions for the NanoWalker robot. In: SPIE2000

14. Wörn H, Schmoeckel F, Buerkle A, Samitier J, Puig-Vidal M, Johansson S, Simu U, Meyer JU, Biehl M (2001) From decimeter to centimeter-sized mobile microrobots. The development of the MINIMAN system. In: Conference on microrobotics and microassembly III

15. Burisch A, Soetebier S, Wrege J, Hesselbach J (2004) Piezoelectric stick-slip-actuator with normal-force-modulation. In: Actuator2004, 9th international conference on new actuators, Bremen, Germany

16. Snis N, Simu U, Johansson S (2004) Piezoelectric drive platform for cm^3-sized autonomous robot. In: Actuator2004, 9th international conference on new actuators, Bremen, Germany

17. Bergander A, Driesen W, Varidel T, Breguet JM (2004) Monolithic piezoelectric actuators for miniature robotic systems. In: Actuator2004, 9th international conference on new actuators, Bremen, Germany

18. Breguet JM, Johansson S, Driesen W, Simu U (2006) A review on actuation principles for few cubic millimeter sized mobile micro-robots. In: Actuator2006, 10th international conference on new actuators, Bremen, Germany

19. Driesen W, Breguet JM, Clavel R (2006) Novel locomotion principles for mobile micro robots. In: Actuator2006, 10th international conference on new actuators, Bremen, Germany

20. Floyd S, Pawashe C, Sitti M (2008) An untethered magnetically actuated micro-robot capable of motion on arbitrary surfaces. In: IEEE international conference on robotics and automation

21. Jasper D, Edeler C (2008) Characterization, optimization and control of a mobile platform. In: International workshop on microfactories, IWMF

22. Edeler C (2011) Measurements and potential applications of force-control method for stick-slip-driven nanohandling robots (accepted). In: International conference on materials, mechatronics and automation

23. Murthy R, Popa DO (2009) A four degree of freedom microrobot with large work volume. In: IEEE international conference on robotics and automation

24. Peng JY, Chen DB (2010) Modeling of piezoelectric-driven stick–slip actuators. IEEE/ASME Trans Mechatron 99:1

25. Patrascu M, Stramigioli S (2007) Modeling and simulating the stick-slip motion of the μWalker, a MEMS-based device for μSPAM. Microsyst Technol 13(2):181–188

26. Zesch W, Buechi R, Codourey A, Siegwart RY (1995) Inertial drives for micro- and nanorobots: analytical study. In: Proc. SPIE

27. Breguet JM (1998) Stick and slip actuators. PhD thesis, École Polytechnique Fédérale de Lausanne EPFL, Switzerland

28. Altpeter F (1999) Friction modeling, identification and compensation. PhD thesis, École Polytechnique Fédérale de Lausanne EPFL, Switzerland

29. Bergander A (2003) Control, wear and integration of stick-slip micropositioning. Thesis no 2843, École Polytechnique Fédérale de Lausanne EPFL, Lausanne, Switzerland

30. Driesen W (2008) Concept, modeling and experimental characterization of the modulated friction inertial drive (MFID) locomotion principle. PhD thesis, École Polytechnique Fédérale de Lausanne EPFL, Lausanne, Switzerland

31. de Wit CC, Olsson H, Astrom KJ, Lischinsky P (1995) A new model for control of systems with friction. IEEE Trans Automat Contr 40:419–425

32. Heslot F, Baumberger T, Perrin B, Caroli C (1994) Creep, stick-slip, and dry-friction dynamics: experiments and a heuristic model. Phys Rev E 49(6):4973–4988

33. Edeler C, Meyer I, Fatikow S (2010) Simulation and measurements of stick-slip-microdrives for nanorobots. In: European conference on mechanism science, EUCOMES

34. Edeler C, Fatikow S (2011) Open loop force control of piezo-actuated stick-slip drives. International journal on intelligent mechanisms and robots 1(1):1–19

35. Popov VL (2009) Kontaktmechanik und Reibung (German). Springer

36. Ogilvy JA (1991) Numerical simulation of friction between contacting rough surfaces. J Phys D, Appl Phys 24:2098–2109

37. Karnopp D (1985) Computer simulation of stick-slip friction in mechanical dynamic systems. J Dyn Syst Meas Control 107(1):100–103

38. Mariotto G, D'Angelo M, Shvets IV (1999) Dynamic behavior of a piezowalker, inertial and frictional configurations. Rev Sci Instrum 70:3651–3655

39. Edeler C (2008) Simulation and experimental evaluation of laser-structured actuators for a mobile microrobot. In: Proceedings of IEEE international conference on robotics and automation

40. Dupont P, Armstrong B, Hayward V (2000) Elasto-plastic friction model: contact compliance and stiction. In: Proceedings of the American control conference Chicago

41. Dupont P, Hayward V, Armstrong B, Altpeter F (2002) Single state elastoplastic friction models. IEEE Trans Automat Contr 47:787–792

42. Dahl PR (1968) A solid friction model. Tech. rep., Aerospace Corp el Segundo CA

43. Kogut L, Etsion I (2004) A static friction model for elastic-plastic contacting rough surfaces. Trans ASME 126:34–40

44. Chang WR, Etsion I, Bogy DB (1987) An elastic-plastic model for the contact of rough surfaces. J Tribol 109(2):257–263

45. Rabinowicz E (1958) The intrinsic variables affecting the stick-slip process. Proc Phys Soc 71(4):668

46. Urbakh M, Klafter J, Gourdon D, Israelachvili J (2004) The nonlinear nature of friction. Nature 430(29):525–528

47. Persson BNJ (1993) Theory and simulation of sliding friction. Phys Rev Lett 71(8):1212–1215

48. Bowden FP, Tabor D (1986) The friction and lubrication of solids. Clarendon Press, Oxford

49. Armstrong-Hélouvry B, Dupont P, de Wit C (1994) A survey of models, analysis tools and compensation methods for the control of machines with friction. Automatica 30(7):1083–1138

50. Yeh R, Pister KSJ (1995) Measurement of static friction in mechanical couplings of articulated microrobots. In: Symposium on micromachining and microfabrication

51. Dieterich JH (1978) Time-dependent friction and the mechanics of stick-slip. Pure Appl Geophys 116:790–806

J. Micro-Nano Mech. (2011) 6:65–87

87

52. Piedboeuf JC, Carufel JD, Hurteau R (2000) Friction and stick-slip in robots: simulation and experimentation. Multibody Syst Dyn 4:341–354
53. Johnson KL, Woodhouse J (1998) Stick-slip motion in the atomic force microscope. Tribol Lett 5:155–160
54. Bhushan B, Israelachvili JN, Landmann U (1995) Nanotribology: friction, wear and lubrication at the atomic scale. Nature 374:607–616
55. Hertz H (1826) Über die Berührung fester elastischer Körper, (German). J Reine Angew Math 92:156–171
56. Hartikainen J, Kolar K, Kouhia R (2010) A constitutive model for strain-rate dependent ductile-to-brittle transition. In: 23rd nordic seminar on computational mechanics
57. Durst K, Goken M (2004) Nanoindentierung - eine Sonde für die lokalen mechanischen Eigenschaften (German). Sonderbd Prakt Metallogr 36:319–328
58. Greenwood JA, Williamson JBP (1966) Contact of nominally flat surfaces. Proc R Soc Lond, A Math Phys Sci 295(1442):300–319
59. Bergander A, Breguet JM (2003) Performance improvements for stick-slip positioners. In: Proc. int. symposium on micromechatronics and human science (MHS'03), Nagoya, Japan, pp 59–66
60. Singer NC, Seering WP (1988) Preshaping command inputs to reduce system vibration. Massachusetts Institute of Technology, Artificial Intelligence Laboratory
61. Murphy BR, Watanabe I (1992) Digital shaping filters for reducing machine vibration. IEEE Trans Robot Autom 8(2):285–289
62. Mindlin RD (1949) Compliance of elastic bodies in contact. J Appl Mech 16:259–268
63. Landolsi F, Ghorbel FH, Lou J, Lu H, Sun Y (2009) Nanoscale friction dynamic modeling. J Dyn Syst Meas Control 131(6):061102
64. PI Ceramic GmbH (2010) Lindenstraße, 07589 Lederhose, Germany. http://www.piceramic.de
65. Adriaens HJMTA, de Koning WL, Banning R (2000) Modeling piezoelectric actuators. IEEE Trans Mechatron 5(4): 331–341
66. Chonan S, Jiang Z, Yamamoto T (1996) Nonlinear hysteresis compensation of piezoelectric ceramic actuators. J Intell Mater Syst Struct 7(2):150–156
67. Rabinowicz E (1995) Friction and wear of materials. Wiley
68. Blok H (1955) The dissipation of frictional heat. Appl Sci Resource 5(Section A):151–181
69. Bowden FP, Freitag EH (1958) The friction of solids at very high speeds. Proc R Soc Lond, A Math Phys Sci 248(1254): 350–367
70. Budakian R, Putterman SJ (2000) Correlation between charge transfer and stick-slip friction at a metal-insulator interface. Phys Rev Lett 85(5):1000–1003
71. Littmann W, Storck H, Wallaschek J (2001) Sliding friction in the presence of ultrasonic friction: superposition of longitudinal oscillations. Arch Appl Mech 71:549–554
72. Lübke M (2010) Aufbau eines Reibkraftmessstandes und Durchführung von Messreihen (German). Student research project, University of Oldenburg
73. Bowden FP, Tabor D (1949) The seizure of metals. Proc Inst Mech Eng 160:380–383
74. Smith ST, Chetwynd DG (1992) Foundations of ultraprecision mechanism design. Gordon and Breach Science Publishers